Tuning the Inclusion Properties and Solid-State Reactivity of Second Sphere Adducts Using Conformationally Flexible Bidentate Ligands

Fang Guo,*[,†] Xu Wang,[†] Hong-yu Guan,[†] Hai-bin Yu,[†] Lei Li,[†] Shan-shan Chen,[†] Antonino Famulari,[‡] and Javier Martí-Rujas*[,§]

[†]College of Chemistry, Liaoning University, Shenyang 110036, China

[‡]Dipartimento di Chimica Materiali e Ingegneria Chimica. "'Giulio Natta"', Politecnico di Milano, Via L. Mancinelli 7, 20131 Milan, Italy

[§]Center for Nano Science and Technology@Polimi, Istituto Italiano di Tecnologia, Via Pascoli 70/3, 20133 Milano, Italy

Received: February 24, 2015
Revised: May 1, 2015
Published: May 11, 2015

Corresponding Authors

*E-mail: fguo@lnu.edu.cn.
*E-mail: javier.rujas@iit.it.

INTRODUCTION

Chemical reactions carried out in the solid state induced by external stimuli are important to gain insight on how chemical reactions occur.[1−10] An important aspect is on the ability to bring the reacting molecules into an optimal orientation and distance allowing the reaction partners to interact and react. Molecular recognition is crucial to bring the reactants together, but such control is often difficult in the solid-state. Crystal engineering is one of the most important routes to achieve molecular recognition by proper combination of functional groups present in molecules or ions.[11,12] One way to achieve selectivity and effective binding of ions can be obtained by using the concept of second sphere coordination.[13]

Second sphere coordination was described by Alfred Werner over a century ago by describing how the first coordination sphere of a transition metal complex can interact with neutral or charged species to give a second sphere coordination. In the early 80s, studies aimed to get insights into the nature of second sphere coordination were carried out[14−17] and more recently has been exploited to study metal-based anion receptors.[18−20] The first sphere ligands can form second-sphere adducts with the whole range of noncovalent bonding interactions, such as electrostatic, hydrogen bonding, halogen

bonding, charge transfer, and van der Waals interactions. The contribution of second sphere coordination has been important in supramolecular chemistry,[21] including biological recognition.[22]

Solid-state chemistry knowledge of hybrid metal organic compounds (i.e., self-assembled via electrostatic interactions) is very important in order to design new functional materials. However, the solid state chemistry of second sphere coordination has not been studied very much. Only recently, has second sphere coordination been demonstrated that it is a suitable approach to synthesize functional materials for gas adsorption,[23] separation of metal ions[24−27] for the extraction of auric anions using α-cyclodextrin,[28] to study solid-state mechanochemical dehydrochlorination reactions,[29] crystalline-to-polycrystalline reactions,[30] and to form permanent porous networks showing single-crystal-to-single-crystal guest exchange and ionic conductivity.[31] Halogen bonds have been used in second-sphere coordination complexes to form 6,3-networks.[32]

Using large and flexible molecules having bulky groups can be a good crystal engineering strategy to synthesize new host−guest systems[33] because such molecules would not organize efficiently, and therefore, alternative crystal packing modes (using molecule's flexibility) might be achieved by inclusion of guests with good size and shape complementarity.[34]

Our recent research has focused on the construction of a new type of supramolecular inclusion system that cooperatively utilizes secondary sphere coordination interactions, in which a series of *N*-bidentate flexible ligands have been designed as second-sphere ligands and self-assembled with tetrahedral anions like $[MCl_4]^{2-}$ (M = Cu, Co, Mn, and Zn) as the primary coordination sphere.[35] Herein, we have used bibenzylamine ($\mathbf{L^0}$) as an organic moiety, to which we introduced $-(CH_2)_n-$ (n = 1, 2, 3, and 4) alkyl chains on the bibenzylamine ligand to synthesize a series of ligands $\mathbf{L^1}$−$\mathbf{L^4}$ differing only in the backbone chain separating the two aromatic moieties (Scheme 1).

The two N atoms in the flexible backbone can be protonated. They can act as hydrogen-bonding donors (outer sphere), playing a key role in the anion recognition of the primary coordination sphere of tetrachlorometallates such as $[MCl_4]^{2-}$ but also might act as an anchoring point for guests molecules. Moreover, the bulky phenyl rings may also act as molecular recognition site and contribute to the formation of voids to accommodate small/medium guests such as methanol, ethanol, acetic acid, acrylic ester, or acetonitrile. In some complexes, the host structure upon heating is robust enough to allow guest release/uptake while maintaining their crystallinity or via an amorphous phase. Up to now, studies of inclusion complexes involving thermal stability, solid-state mechanochemical dehydrochlorination reactivity, and their guest behavior self-assembled via second-sphere coordination using bidentate ligands with different backbone lengths [i.e., the effect of $-(CH_2)_n-$ spacers] are uncommon. Additionally, we provide quantum mechanical calculations (QM), including methods for solid phases, which have been carried out to gain information about the electronic density distribution of frontier molecular orbitals (FMOs) in ligands $\mathbf{L^2}$−$\mathbf{L^4}$ in order to better understand their solid-state reactivity. The QM results indicate that the orientation and symmetry of the HOMOs (which results were concentrated mainly at the N atoms) need to be considered as well as the backbone N−$(CH_2)_n$−N distance in order to achieve dehydrochlorination reactions followed by chelation upon mechanochemical grinding.

Scheme 1. (a) Ligands Used in This Work and (b) Cartoon Showing the Metals Used As First Coordination Sphere Which are Self-Assembled with Ligands $\mathbf{L^{1-4}}$ via Second Coordination Sphere Interactions

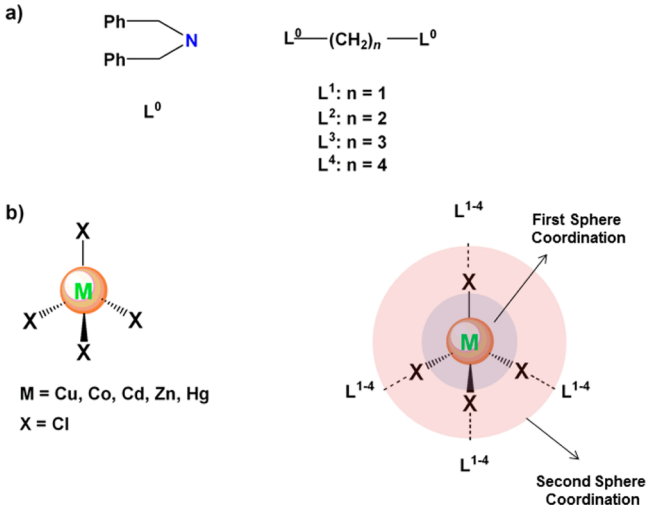

EXPERIMENTAL SECTION

Materials and Methods. All chemicals were obtained from commercial sources and used without further purification. IR spectra were obtained with a PerkinElmer 100 FT-IR spectrometer using KBr pellets. ^{1}H NMR spectra were recorded on a Mercury-Plus 300 spectrometer (VARIAN, 300 MHz) at 25 °C with TMS as the internal reference. Powder X-ray diffraction were recorded using a D8 Bruker and D2 PHASER diffractometer (λ = 1.54056 Å).

Synthesis of Ligands $\mathbf{L^1}$−$\mathbf{L^4}$. *Synthesis of L^1.* For the synthesis of $\mathbf{L^1}$, 8 g (0.04 mol) of bibenzylamine were added into 40 mL of ethanol and slowly stirred at 40 °C. Subsequently, 1.62 g [(0.02 mol) 37% purity] formaldehyde was then continuously (2−3 drops) added into the mixture solution. The reaction was stirred for 2 h, and the mixture was cooled to room temperature. The white product was separated from ethanol and then washed with distilled water. Recrystallization using anhydrous ethanol dried under vacuum conditions produced a white crystalline solid 6.8982 g, yield 84.95%, mp 101−103 °C. ^{1}H NMR ($CDCl_3$, 300 MHz): δ 3.09 (2H, s, CH_2); 3.61 (8H, s, CH_2); and 7.22−7.33 (20H, m, ArH).

Synthesis of L^2. The synthesis of $\mathbf{L^2}$ was carried out by slowly adding 7 mL of ethylene diamine into a solution of 8 g of NaOH and 20 mL of distilled water. Then 30 mL of benzyl chloride (2−3 drops) were continuously added into the mixture solution. The reaction was heated to 95 °C and stirred for 4 h, and then the mixture was cooled to room temperature. The white product was separated from diethyl ether and then washed with distilled water. Recrystallization using anhydrous ethanol dried under vacuum conditions resulted in white crystals 12.43 g, yield 60.0%, and mp 92−95 °C. ^{1}H NMR ($CDCl_3$, 300 MHz): δ 2.60 (4H, s, CH_2), 3.50 (8H, s, CH_2), 7.23−7.28 (20H, m, Ar−H).

Synthesis of L^3. Ligand $\mathbf{L^3}$ was prepared by adding 4.2 mL of 1,3-propanediamine into a solution of 8 g of NaOH and 18 mL of anhydrous ethanol. Then, 27.5 mL of benzyl chloride (2−3 drops/s) were continuously added into the solution. The reaction was heated to 80 °C and stirred for 4 h then cooled to room temperature. The white product was separated from ethanol and then washed with distilled water several times. Recrystallization using anhydrous ethanol dried in vacuum conditions produced white needle crystals 14.06 g, yield 64.6%, and mp 50−51 °C. ^{1}HNMR ($CDCl_3$, 300 MHz): δ 1.71 (2H, s, CH_2), 2.38−2.42 (4H, t, CH_2), 3.48 (8H, s, CH_2), and 7.21−7.28 (20H, m, Ar−H).

Synthesis of L^4. The synthesis of L^4 was performed by adding 2 mL of 1,4-butanediamine into a solution of 7 g $NaHCO_3$ and 20 mL of distilled water. Then, 10 mL benzyl chloride (2−3 drops) were continuously added into the solution. The reaction was heated to 95 °C and stirred for 8 h and cooled to room temperature. The white reaction product was separated from the mixture solution and washed with ethanol and distilled water several times. Drying in a vacuum produced white needle crystals 4.87 g, yield 54.4%, mp 138−140 °C. ^{1}HNMR (DMSO, 300 MHz): δ 1.39 (4H, s, CH_2), 2.25 (4H, s, CH_2), 3.45 (8H, s, CH_2), 7.20−7.30 (20H, m, Ar−H).

Synthesis of $[L^0]2H^+\cdot[CuCl_4]^{2-}$ (1). 0.050 g of (0.00012 mol) L^0 and 5 mL of ethanol were placed in a 50 mL Erlenmeyer flask then 0.5 mL of concentrated hydrochloric acid and 0.050 g (0.00029 mol) of $CuCl_2\cdot 2H_2O$ were slowly added and shaken until the contents were dissolved. The flask was allowed to stand for 1 week at room temperature, giving rise to blue block crystal **1**. Mp: 193−195 °C.

Synthesis of $CH_3CH_2OH\subset[L^2]2H^+\cdot[CuCl_4]^{2-}$ (2). 0.35 g (0.00083 mol) of L^2 and 10 mL of ethanol were placed in a 50 mL Erlenmeyer flask, then 1 mL concentrated hydrochloric acid and 1 mL of prepared $K_2[CuCl_4]$ were added slowly and shaken until the contents were dissolved. The flask was left to stand for about 8−10 days at room temperature, giving rise to orange crystal **2**. Mp: 173−178 °C.

Synthesis of $CH_3OH\subset[L^3]2H^+\cdot[CuCl_4]^{2-}$ (3). 0.10 g (0.00023 mol) of L^3 and 20 mL of methanol were introduced into a 50 mL Erlenmeyer flask, and then 0.19 g of $CuCl_2\cdot 2H_2O$ (0.0011 mol) and 1 mL of concentrated hydrochloric acid were slowly added and shaken until the contents were dissolved. The flask was left for a month at room temperature, giving rise to red block crystals **3**. Mp: 174−185 °C.

Synthesis of $CH_3COOH\subset[L^3]2H^+\cdot[CuCl_4]^{2-}$ (4). 0.10 g (0.00023 mol) of L^3 and 10 mL of acetic acid were placed into a 50 mL Erlenmeyer flask, and then 0.10 g of $CuCl_2\cdot 2H_2O$ (0.00059 mol) and 2 mL of concentrated hydrochloric acid were slowly added and shaken until the contents were dissolved. The flask was allowed to stand for 5 days at room temperature, giving rise to orange-red crystals **4**. Mp: 151−159 °C.

Synthesis of $CH_2CHCOOCH_3\subset[L^3]2H^+\cdot[MCl_4]^{2-}$ (5−7) (M = Zn, Co, Hg). 0.10g (0.00023 mol) of L^3 and 10 mL of acrylic ester were placed into a 50 mL Erlenmeyer flask, and then 0.10 g $ZnCl_2$ (0.00073 mol) and 2 mL of concentrated hydrochloric acid were slowly added and shaken until the contents were dissolved. The flask was left for about 1 week at room temperature, giving rise to transparent block crystals **5**. Mp: 244−255 °C. The same experiments were carried out using $CoCl_2\cdot 6H_2O$/$HgCl_2\cdot 2H_2O$ yielding crystals **6** (mp: 240−244 °C) and **7** (mp: 163−173 °C).

Synthesis of $CH_3CN\cdot H_2O\subset[L^4]2H^+\cdot[MCl_4]^{2-}$ (8−9) (M = Hg, Co). 0.10 g (0.00022 mol) of L^4 and 4 mL of dichloromethane and 20 mL acetonitrile were placed into a 50 mL Erlenmeyer flask, and then 0.10 g $HgCl_2$ (0.00037 mol) and 1 mL concentrated hydrochloric acid were slowly added and shaken until the contents were dissolved. The flask was allowed to stand overnight at room temperature, giving rise to transparent block crystals **8**. Mp: 106−115 °C. The same experiments were carried out using $CoCl_2\cdot 6H_2O$ to produce blue block crystals **9**. Mp: 98−106 °C.

Synthesis of $CH_3OH\subset[L^4]2H^+\cdot[CdCl_4]^{2-}$ (10). 0.10 g (0.00022 mol) of L^4 and 4 mL of dichloromethane and 20 mL methanol were placed into a 50 mL Erlenmeyer flask, and then 0.10 g of $CdCl_2\cdot 2.5H_2O$ (0.00044 mol) and 1 mL of concentrated hydrochloric acid were slowly added and shaken until the contents were dissolved. The flask was allowed to stand overnight at room temperature, giving rise to transparent crystals **10**. Mp:102−107 °C.

Crystallography. Single crystal data collection were performed on a Bruker P4 diffractometer with Mo Kα radiation (λ = 0.71073 Å) and Bruker X8 Prospector APEX-II/CCD diffractometer equipped with a microfocusing mirror (Cu Kα radiation, λ = 1.54056 Å). The structures were determined using direct methods and refined (based on F2 using all independent data) by full-matrix least-squares methods (SHELXTL 97). Data were reduced by using Bruker SAINT. All nonhydrogen atoms were directly located from different Fourier maps and refined with anisotropic displacement parameters. Guest molecules were well-resolved but disordered, with the thermal displacement parameters of some atoms being relatively large, partly owing to the loose packing in the void and partly because the atomic positions represent an average between the included guest molecules. The details of data collection, data reduction, and crystallographic data are summarized in Tables S1 and S2 of the Supporting Information.

Mecanochemistry. Liquid-assisted grinding (LAG) of 32 mg (0.047 mmol) of crystals **3** and 10.5 mg (0.094 mmol) of KOH in a 1:2 molar ratio, with the addition of 30 μL of EtOH was performed. Upon grinding, a color change from orange to brown was observed within 5 min. Then the powder after grinding was recrystallized in anhydrous methanol.

Liquid-assisted grinding (LAG) of 29 mg (0.041 mmol) of crystals **10** and 4.6 mg (0.082 mmol) of KOH in a 1:2 molar ratio, with the addition of 30 μL of anhydrous methanol was carried out. Upon grinding, a color change from colorless to white was observed within **10** min. Then the powder after grinding was recrystallized in anhydrous methanol.

RESULTS AND DISCUSSION

Structure Description of Complexes using L^0 and L^2: Second Sphere Adducts 1 and 2. In the absence of alkyl chain on the bibenzylamine ligand (L^0), the bibenzylamine can directly react with $[CuCl_4]^{2-}$ anion to produce the second-sphere coordination complex $[L^0]2H^+\cdot[CuCl_4]^{2-}$ (**1**). Crystal structure analysis reveals that the asymmetric unit in **1** comprises half $[CuCl_4]^{2-}$ anion and one diprotonated L^0 ligand. The $[CuCl_4]^{2-}$ anion adopts planar geometry, with the Cu−Cl bond lengths being 2.245 (1) Å and 2.279 (1) Å, respectively. Each $[CuCl_4]^{2-}$ anion is surrounded by four protonated L^0 through N−H···Cl interactions (i, ii) and expanded into a linear hydrogen bonding chain along the crystallographic *a* axis (Figure 1). The second sphere adduct **1** does not include guest molecules.

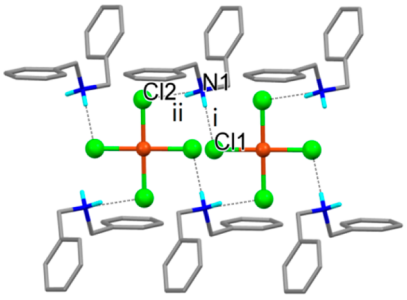

Figure 1. Crystal structure of **1** showing the second-sphere coordination formed by L^0 and $[CuCl_4]^{2-}$ anions. N−H···Cl interactions (i, ii) showed as dashed lines.

Using L^1 (one $-CH_2-$ spacer), no second sphere adduct was obtained. In fact, the reaction between L^1 and $[MCl_4]^{2-}$ showed that the ligand L^1 is unstable and decomposes into L^0 and subsequently forms complexes with $[MCl_4]^{2-}$.

However, when the $N-CH_2-N$ backbone was expanded by introducing an extra CH_2 group to form the $-(CH_2)_2-$ backbone, the ligand L^2 was obtained. X-ray crystallography reveals that L^2 crystallized in the $P\bar{1}$ space group with half molecule in the asymmetric unit.[36] The intramolecular N···N distance is 3.766 Å. The diffusion of $CuCl_2\cdot 2H_2O$ in EtOH into a HCl/EtOH solution of L^2 resulted in the second sphere adduct **2**, in which the host framework $[L^2]2H^+\cdot[CuCl_4]^{2-}$ includes EtOH guest molecules. Single crystal XRD shows that there are two $[CuCl_4]^{2-}$ dianions, two doubly protonated L^2 and one EtOH molecules in each asymmetric unit. The two

protons in L^2 are linked with the same $[CuCl_4]^{2-}$ anion through two charge-assisted N−H···Cl hydrogen bonds (i, ii), giving rise to a *quasi*-chelating[37] building block **1** (Figure 2a).

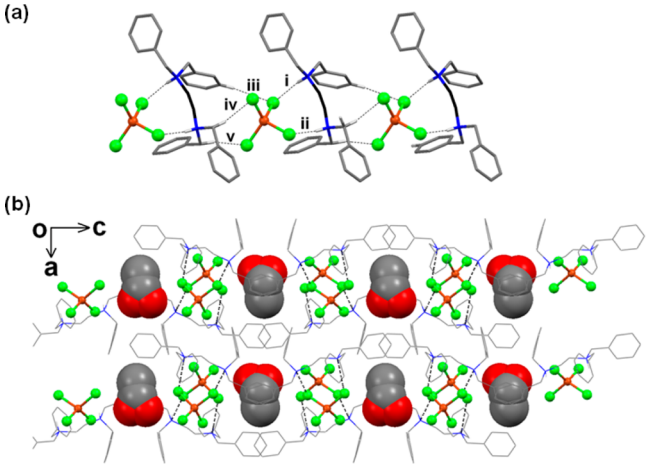

Figure 2. (a) Crystal structure of **2** showing the *quasi*-chelating hydrogen-bonded chain along the *b* axis via C−H···Cl interactions. (b) View along the *c* axis of the included ethanol molecules (spacefilling) disordered over two positions.

The geometry of the $[CuCl_4]^{2-}$ anion forms a highly distorted tetrahedral coordination environment with Cl atoms. The neighboring *quasi*-chelating building blocks further form a hydrogen-bonded chain along the crystallographic *b* axis through C−H···Cl interactions (Figure 2a, panels iii−v) and then expanded into a cagelike along *c*-axis accommodating disordered ethanol (i.e., over two positions) guest molecules (Figure 2b).

Structure Description of Complexes Using L^3: Second Sphere Adducts 3−7. *Structure Description of $CH_3OH\subset[L^3]2H^+\cdot[MCl_4]^{2-}$ (**3**).* The insertion of an extra methylene in L^2 formed a new ligand (L^3). From single crystal X-ray diffraction data, we observed that the intramolecular N··· N distance increased from 3.766 Å in L^2 to 5.113 Å in L^3.[37] The diffusion of a methanolic solution of $CuCl_2{\cdot}2H_2O$ into the HCl/MeOH solution of L^3 gave good quality single crystals of the second sphere adduct $CH_3OH\subset[L^3]2H^+\cdot[CuCl_4]^{2-}$ (**3**). X-ray crystallographic analysis reveals that **3** is monoclinic ($P2_1/c$) with one dianion $[CuCl_4]^{2-}$, one doubly protonated L^3, and one methanol molecule in the asymmetric unit. One double-protonated ligand L^3 is linked with two different $[CuCl_4]^{2-}$ anions through N−H···Cl interactions (i, ii), forming the nonchelating dication−dianion building block which propagates along the *b* axis (Figure 3a). Methanol molecules are trapped in the concave region of the helical chain through the O−H···Cl interaction [3.165(4) Å] involving the hydroxyl groups and chloride atoms of $[CuCl_4]^{2-}$ anions. The helical chains are linked further by weak C−H···Cl hydrogen bonds (iii−v) along the *c* axis, constructing a 3D structure (Figure 3b).

We note that **3** is not isostructural to other two second sphere adducts crystallized using L^3 $[HgCl_4]^{2-}$ and $[ZnCl_4]^{2-}$, which also include methanol as a guest.[37] This demonstrates the structural diversity of this type of second sphere complexes (Figure 4, panels a−c).

*Structure Description of $CH_3COOH\subset[L^3]2H^+\cdot[CuCl_4]^{2-}$ (**4**).* It is known that weak interactions are crucial in the molecular self-assembling outcome. The effect of the solvent molecules can direct the crystallization affecting the stoichiometric ratio

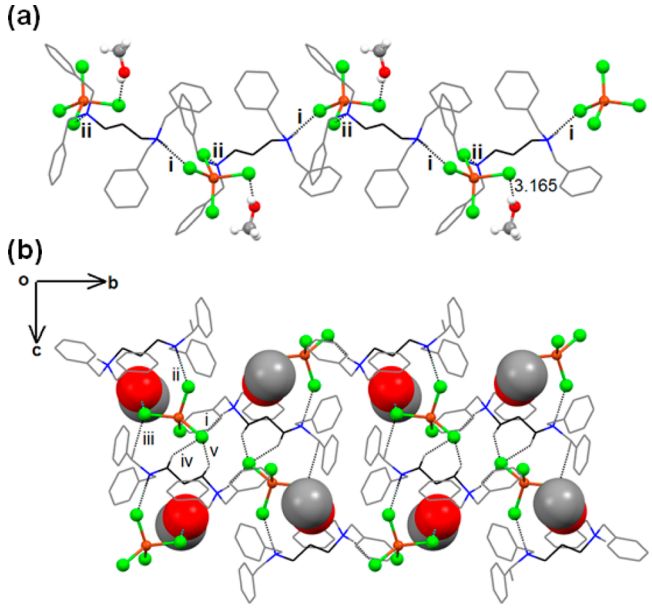

Figure 3. (a) View along the *b* axis of the hydrogen-bonding interactions (dashed lines) between dianions, dications, and solvent in **3**. (b) View of the crystal packing of **3** accommodating methanol guest molecules.

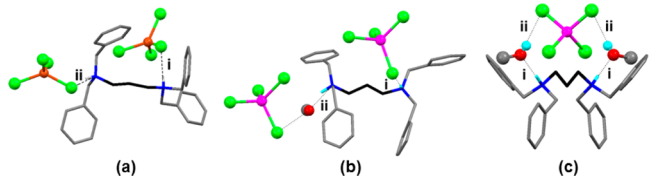

Figure 4. Different building blocks in crystals formed by L^3 and metal chlorides in MeOH solvent: (a) crystal **3**; (b) different building blocks previously reported in second sphere adducts (b) and (c).

between the self-assembling building blocks (i.e., cations, anions, and solvent molecules in this case). The following example is a proof on how by replacing methanol for acetic acid in the crystallization of L^3 and $[CuCl_4]^{2-}$ results in a completely different second sphere adduct. This adduct was synthesized diffusing $CuCl_2{\cdot}2H_2O$ in acetic acid into a HCl/MeOH solution containing ligand L^3 to yield the salt $CH_3COOH\subset[L^3]2H^+\cdot[CuCl_4]^{2-}$ (**4**). The metal organic hybrid complex **4** crystallizes in the monoclinic system in the $P2_1/c$ space group, with two independent doubly protonated L^3 ligands, two $[CuCl_4]^{2-}$ dianions, and one acetic acid in the asymmetric unit.

The two independent L^3 ligands (labeled L^{3a}, L^{3b}) in the asymmetric unit interact with two independent $[CuCl_4]^{2-}$ dianions ($[CuCl_4]^{2-}{}_a$,$CuCl_4]^{2-}{}_b$) through N−H···Cl interactions, constructing two individual building blocks (Figure 5a). In one of the building blocks, one ligand L^{3a} is connected with two independent $[CuCl_4]^{2-}$ anions ($[CuCl_4]^{2-}{}_a$,$CuCl_4]^{2-}{}_b$) through N−H···Cl interactions (i and ii), whereas in the other building block, the other ligand L^{3b} and the $[CuCl_4]^{2-}{}_a$ anion via four N−H···Cl interactions (iii and iv) as shown in Figure 5a. The building blocks are alternately arranged along the *c* axis through C−H···Cl weak interactions (v−ix) to build a 3D structure (Figure 5b), with acetic acid guest molecules filling the concave region through O−H···Cl interactions (3.148 Å).

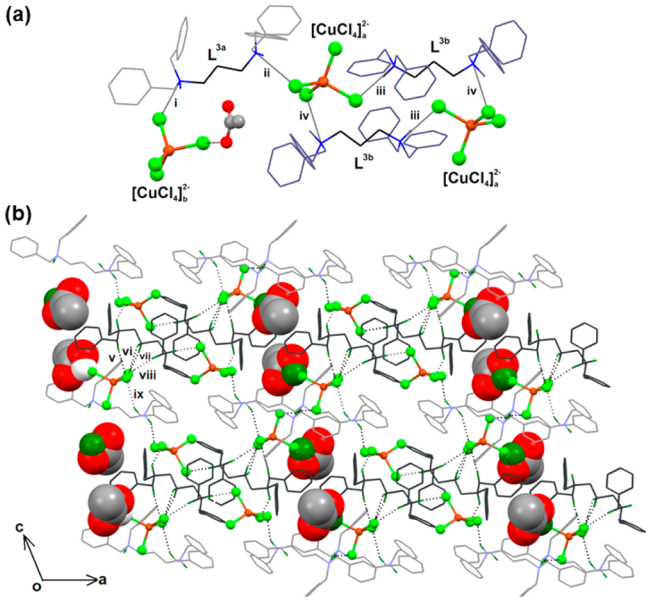

Figure 5. (a) Crystal structure of **4** showing the two different building blocks involving L^{3a} and L^{3b}. Crystal packing in **4** showing the inclusion of acetic acid as guest molecule (spacefilling).

*Structure Description of $CH_2CHCOOCH_3\subset[L^3]2H^+\cdot[MCl_4]^{2-}$ (**5**–**7**).* In order to test the guest inclusion ability of the second sphere adducts self-assembled using L^3, we used larger guest molecules such as acrylic ester. When acrylic ester was added into a mixture of a solution of $HgCl_2\cdot2H_2O/ZnCl_2\cdot2H_2O/CoCl_2\cdot2H_2O$ and L^3 in HCl/EtOH, the $CH_2CHCOOCH_3\subset[L^3]2H^+\cdot[MCl_4]^{2-}$ [M = Zn (**5**); M = Co (**6**), M = Hg (**7**) inclusion complexes were formed]. Since **5**–**7** are isostructural, the description of one (Zn) of the structures will suffice for all. The crystal structure of **5** crystallizes in the monoclinic $P2_1/n$ space group, with one doubly protonated L^3, one $[ZnCl_4]^{2-}$ dianion, and half acrylic ester in each asymmetric unit. Each two L^3 ligands and two $[ZnCl_4]^{2-}$ dianions form a closed hydrogen-bonded network through four N–H···Cl hydrogen bonds (i, ii), forming the building block (Figure 6a). The neighboring building blocks are arranged nearly perpendicular, giving a linear hydrogen-bonded chain through weak C–H···Cl interactions (iii–vi) (Figure S2 of the Supporting Information and Figure 6b) and further expanded into a 3D structure, in which the acrylic ester adopts planar conformation and is accommodated inside the host framework formed by L^3 and $[MCl_4]^{2-}$ dianions through C–H···O interaction [3.070(3) Å]. For the isostructural $[HgCl_4]^{2-}$ and $[CoCl_4]^{2-}$ second sphere adducts, see the Supporting Information.

Structure Description of Complexes Using L^4: Second Sphere Adducts 8–10. *Structure Description of $CH_3CN\cdot H_2O\subset[L^4]2H^+\cdot[MCl_4]^{2-}$ (**8**–**9**).* To explore the guest behavior of this family of flexible molecules, we synthesized a new bidentate ligand L^4 with a longer $-(CH_2)_4-$ backbone chain and, therefore, higher conformational flexibility. The X-ray crystal structure shows that in the asymmetric unit there is a half molecule of L^4. The molecule crystallizes in the $P\bar{1}$ space group. The $N-(CH_2)_4-N$ distance increased to 6.266(4) Å to give a longer backbone.

Addition of $HgCl_2/CoCl_2$ in a dichloromethane (DCM) solution containing L^4 and $HCl/CNCH_3$ for 4 days resulted in the isostructural second sphere adducts $CH_3CN\cdot H_2O\subset[L^4]\cdot2H^+\cdot[MCl_4]^{2-}$ [M = Hg, (**8**); M = Co, (**9**)]. The two complexes crystallize in the monoclinic $P2_1/n$ space group, with one doubly protonated L^4, one $[HgCl_4]^{2-}$ dianion, one acetonitrile, and one water molecule in the asymmetric unit. It is an enclosed hydrogen-bonding interaction between L^4 and $[HgCl_4]^{2-}/[CoCl_4]^{2-}$ anion involving water molecules as a linker (Figure 7a).

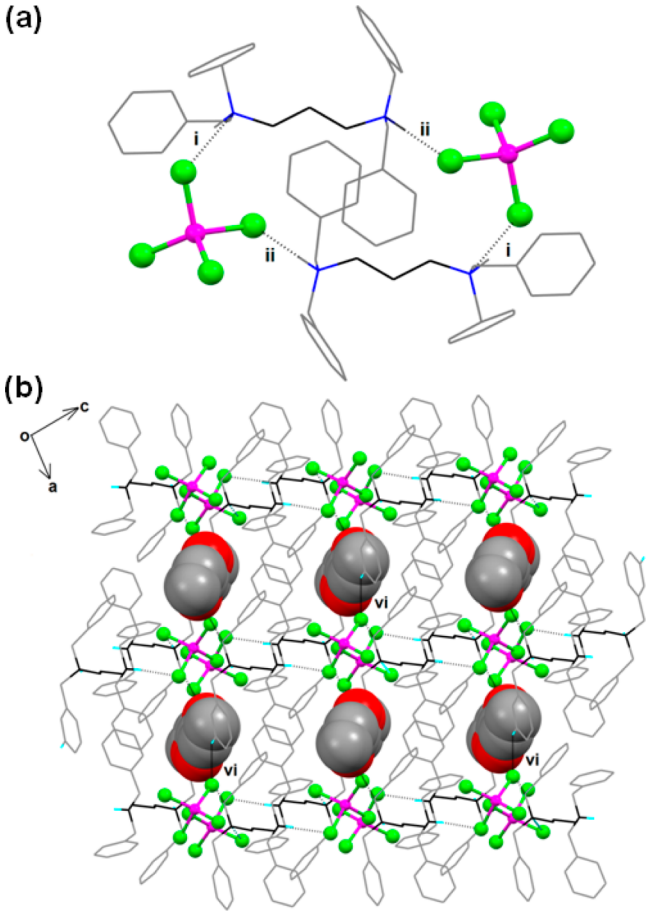

Figure 6. Single crystal structure of second sphere adduct **5**. (a) View of the building block involving dianion and dications. (b) Crystal packing showing the inclusion acrylic ester guest molecules (space-filling).

The second sphere adduct **8** has a building block that involves three types of hydrogen bonds: the expected N–H···Cl interaction between N ligand and $[HgCl_4]^{2-}/[CoCl_4]^{2-}$ (i), N–H···O interaction between ligand and linker water molecules (ii), and O–H···Cl interactions between water and $[HgCl_4]^{2-}$ (iii). The acetonitrile molecule is encapsulated and stabilized by O–H···N interactions (iv) between the other remaining unused hydrogen atom of water and N atom of the CN group. Interestingly, the CH_3CN molecules do not play a primary role in the host hydrogen bond network and are somehow acting as templates to fill the empty space, while water is more directly involved in the host framework, bridging the dication and dianion (Figure 7a). The building blocks are further linked to each other through C–H···Cl interactions (v–viii) along the *b* and *c* axes, constructing a 3D structure as seen in Figure 7b, with the ligand molecules in a helical arrangement along the *c* axis.

*Structure Description of $CH_3OH\subset[L^4]2H^+\cdot[CdCl_4]^{2-}$ (**10**).* Using the above same conditions, the ligand L^4 can react with

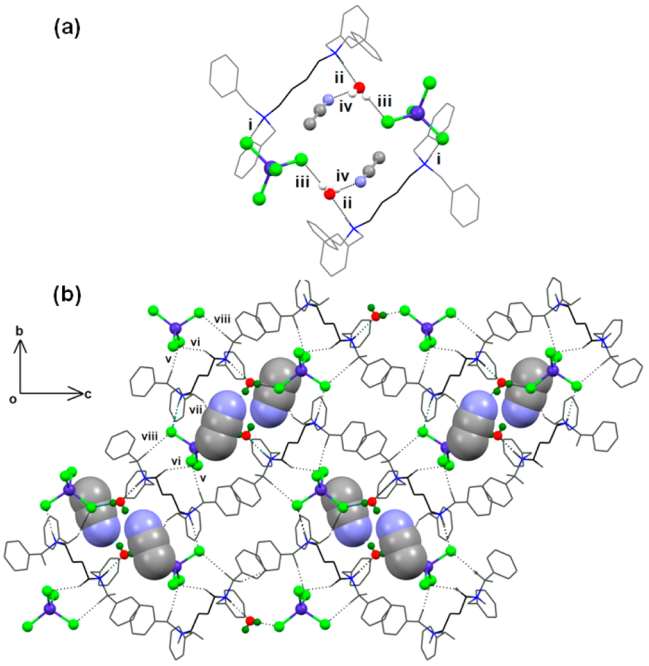

Figure 7. (a) Crystal structure of second sphere adduct **8** showing the main hydrogen bonds between dications and dianions (i.e., the building block). (b) Crystal packing in **8** displaying also the hydrogen bonds between adjacent building blocks (b). The included acetonitrile guest molecules are shown as the spacefilling model.

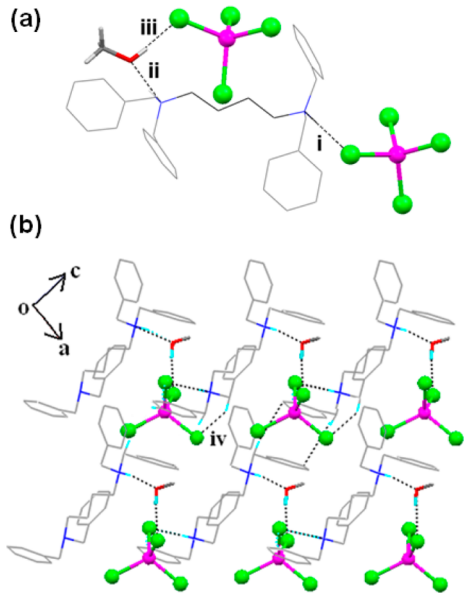

Figure 8. (a) Single crystal structure of **10**. View of the building block involving dication, dianion, and a water guest molecule. (b) Crystal packing showing the hydrogen-bonding interactions perpendicular to the crystallographic *ac* plane (b). Hydrogen bonds are shown as dash lines.

$CdCl_2 \cdot 2.5H_2O$ in methanol to produce the complex $CH_3OH \subset [L^4]2H^+ \cdot [CdCl_4]^{2-}$ (**10**). The complex crystallizes in the monoclinic $P2_1/n$ space group, with one doubly protonated $\mathbf{L^4}$, one $[MCl_4]^{2-}$ dianion, and one methanol in one asymmetric unit. One protonated NH in $\mathbf{L^4}$ is connected with the $[CdCl_4]^{2-}$ dianion through N−H···Cl interaction (i), the other protonated NH in $\mathbf{L^4}$ is linked with the methanol molecule through the N−H···O interaction (ii). Then the methanol acts as a link further connecting with another $[CdCl_4]^{2-}$ dianion through the O−H···Cl hydrogen bonding (iii). The above three hydrogen bonds comprise a new building block. The building blocks are further linked to a linear chain along the diagonal of the *ac* axis (Figure 8a) and then expanded into a 3D structure through C−H···Cl (iv) (Figure 8b).

Influence of $-(CH_2)_n-$ (n = 2, 3, 4) Spacer Lengths for Inclusion Property. The metal:ligand ratio can be an important parameter controlling the dimensionality of the resultant second sphere adduct. Herein, the metal:ligand ratio is constant (1:1) in crystals **2**−**10**. Only **1** formed by the $\mathbf{L^0}$ ligand gives rise to the 1:2 ratio but does not show guest inclusion (i.e., due to the ligand size). The tetrachlorometallate dianion adopts a planar geometry in crystal **1** but forms various distorted tetrahedral $[MCl_4]^{2-}$ dianions in **2**−**10** crystals. The alkyl chain length is an important factor determining the formation of second-sphere coordination giving rise to different guest molecules. Such versatility/flexibility allows keeping the 1:1 metal ratio even if the chain length increases from 3.766 to 6.266 Å.

QM calculations specific for solid state phases, particularly DFT approaches have demonstrated that for the ligand with two methyl groups in the backbone, the stability is higher than that with three methyl groups.[37] Moreover, the conformational freedom introduced by the addition of methylene groups has a strong influence in the conformational flexibility of the ligand when it self-assembles with the metal ions and solvent molecules. In the second sphere adduct **1** containing $\mathbf{L^0}$ (i.e., without alkyl), only one nitrogen donor reacts with the dianion $[CuCl_4]^{2-}$ through N−H···Cl interactions, constructing a linear second sphere adduct without included guests. Interestingly, the ligand $\mathbf{L^1}$ $[-(CH_2)_n- \; n = 1]$ is unstable during the self-assembling reaction with $[MCl_4]^{2-}$ and decomposes into $\mathbf{L^0}$ and subsequently forms crystal **1**.

In $\mathbf{L^2}$, the length between the two nitrogen atoms is ca. 3.76 Å, adopting a gauche conformation in crystal **2** (Figure 9a) and forms a *quasi*-chelating N−H···Cl hydrogen bond with $[MCl_4]^{2-}$, including ethanol in the host framework.

By increasing the methylene chain length $[(CH_2)_n \; (n = 3)]$, the distance between the two nitrogen donors in $\mathbf{L^3}$ is ca. 5.11 Å. $\mathbf{L^3}$ exhibits higher conformational diversity due to the higher flexibility of the ligand. $\mathbf{L^3}$ adopts antiperiplanar conformation or gauche conformation in this crystal (Figure 9, panels b−d). The host framework takes different molecular arrangements to fit the demands of the same guest species (methanol). In **3**, methanol is not directly involved in the connection between the ligand and $[MCl_4]^{2-}$. Additionally, acetic acid or acrylic ester can also be included in the host cavity formed by $\mathbf{L^3}$ and $[MCl_4]^{2-}$, in which $\mathbf{L^3}$ adopts gauche conformation in crystal **4** (Figure 9e) and crystals **5**−**7** (Figure 9f).

With longer methylene chains $[(CH_2)_n \; (n = 4)]$, acetonitrile and methanol molecules were included in the host framework formed by $\mathbf{L^4}$ and $[MCl_4]^{2-}$ and due to length increase of N···N by $(CH_2)_4$ spacer (6.34 Å), the interaction with $[MCl_4]^{2-}$ is through water molecules and acetonitrile. $\mathbf{L^4}$ also exhibits flexibility and can adopt gauche conformation in crystals **8**−**9** (Figure 9g) whereas an antiperiplanar conformation in crystal **10** (Figure 9 h).

Thermal Stability of Supramolecular Adducts 1−10. The thermal stability and the reversible/irreversible properties (guest behavior) of complexes **2**, **4**, and **8** have been studied. The experimental PXRD patterns of complexes **1**−**10** are in

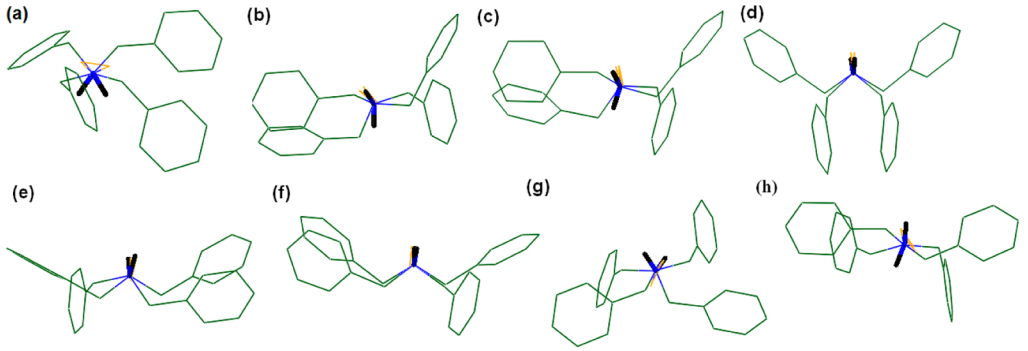

Figure 9. Diversity in the conformations of L^2–L^4 in crystals **2**–**10** viewed from the projection of the Newman-type overlay of two nitrogen atoms: (a) L^2 in crystal **2**; (b) L^3 in crystal **3**; (c,d) L^3 in previous reported crystal structures; (e) L^3 in crystal **4**; (f) L^3 in crystal **5**–**7**; (g) L^4 in crystal **8**–**9**, and (h) L^4 in crystal **10**.

agreement with the simulated diffraction patterns from their respective single crystal structures (Figure S6–S13 of the Supporting Information), thus confirming their phase purity.

To begin with, we monitored the thermal stability of the second sphere adduct **2** which contains L^2. The release of the guest molecules has been monitored first by thermogravimetrical analysis (TGA), which showed that crystal **2** exhibits an initial weight loss (3.4%) from RT to 137 °C, corresponding to the release of ethanol (calcd 3.5%). Further heating leads to the loss of ligand. Second, we have monitored the thermal stability of **2** by heating from RT to 150 °C by holding the sample at 100 °C for several hours. As shown in Figure S14 of the Supporting Information, the crystallinity is practically lost after 15 h at 100 °C but seems that at 120 °C, there is somehow a reorganization as weak diffraction is observed. However, at higher temperatures (i.e., 120–150 °C), the crystallinity is lost and the original crystalline structure (**2**) is not restored after immersing the heated powders of **2** in EtOH for 24 h.

The structural stability of **4**, formed using L^3, was also monitored upon heating. We found that heating complex **4** to 160 °C showed that after 140 °C, an amorphous phase is obtained and did not return to the original structure when it was immersed in acetic acid (Figure S19 of the Supporting Information). The structural transformation is probably too severe to allow the reconstruction of the framework. TG analysis reveals that **4**, the first weight loss (4.57%) from 50 to 170 °C corresponds to the release of acetic acid (calcd 4.46%).

The investigation of reversible guest inclusion/release process of supramolecular second sphere adducts including ligand L^4 and $[MCl_4]^{2-}$ shows an interesting result for the second sphere adduct **8**. The PXRD pattern of **8** shows that the positions and intensities of all peaks shifted upon heating at 100 °C, suggesting that the supramolecular host structure changed upon CH_3CN release while maintaining the crystallinity (see the Supporting Information). Powder XRD indicates that a new phase is obtained at least for that period of heating time (as seen in Figure 10d). Interestingly, when we put the polycrystalline powder in acetonitrile/water for 72 h, the original structure was formed again (Figure 10e).

TGA corroborates that **8**, shows two distinct weight losses corresponding to the CH_3CN and water, respectively. The weight loss (4.90%) fits with the release of CH_3CN molecules from RT to 120 °C (calcd 4.82%) and the subsequent weight loss (2.32%) from 120 to 170 °C corresponds to the release of water molecules (calcd 2.22%). We note that the PXRD pattern

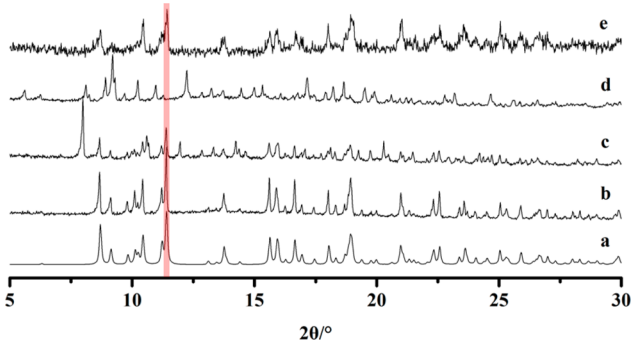

Figure 10. Experimental PXRD patterns of **8**: (a) Simulated PXRD from single crystal; (b) as synthesized PXRD pattern; (c) sample heated at 100 °C for 1 h; (d) sample heated at 100 °C for 3 h; and (e) immersing (d) sample in acetonitrile/water for 100 h. The diffraction peak highlighted in red corresponds to the most intense peak of **8** that does not appear after being heated to 100 °C for 3 h.

obtained after 3 h at 100 °C might be the one corresponding to the structure containing only H_2O (as shown by TG and by the fact that there is no presence of **8** as the most intense peak at ca. 2-theta 12° is not present anymore Figure 10d), and therefore, a stepwise guest release is observed. The restoration of **8** occurs as it might be helped by the presence of H_2O in the crystal structure (Figure 10e).

In order to corroborate the dynamic behavior of adducts including L^4, we have prepared a new second sphere complex that includes ethanol and water as a guest **8·EtOH·H_2O** (see the Supporting Information). We demonstrate that if **8·EtOH·H_2O** is heated up to 100 °C for 1 h, it becomes amorphous upon guest release (i.e., corroborated by ^1H NMR), but if it is immersed again in EtOH, the desolvated adduct reverts to its initial structure as shown by PXRD (Figure 11). Thus, the dynamic behavior in a second sphere adduct is observed following a crystalline-to-amorphous-to-crystalline transformation which is reminiscent to some coordination networks.[9,38–40] Such reconstruction of the original framework is indicative of a certain structural memory retained in the amorphous phase, clearly demonstrating that second sphere coordination adducts can be flexible and active upon external stimuli.

Influence of $-(CH_2)_n-$ (n = 2, 3, 4) Spacer Lengths on the Solid-State Mechanochemical Dehydrochlorination Reaction. Dehydrochlorination reactions consisting of the removal of HCl from crystalline salts are one type of reactions that have been rarely investigated in coordination molecular

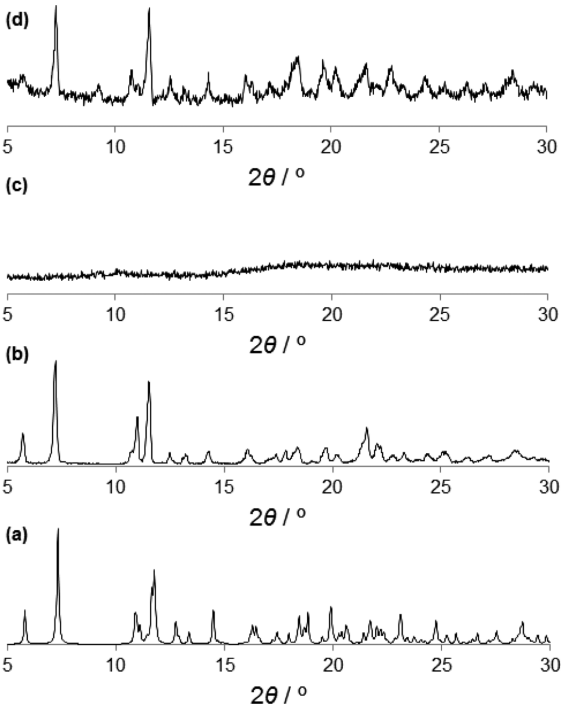

Figure 11. (a) Simulated PXRD (100 K) of **8·EtOH·H_2O**. (b) Experimental PXRD (300 K) of **8·EtOH·H_2O**. (c) PXRD (300 K) corresponding to single crystals of **8·EtOH·H_2O** heated up to 100 °C for 1 h. (d) PXRD of the immersed amorphous phase obtained upon heating **8·EtOH·H_2O** to 100 °C in EtOH for 24 h.

complexes.[41,42] Recently, we have studied the mechanochemical transformation of the second sphere adduct $[L]2H^+\cdot[CuCl_4]^{2-}$ (L = *N,N,N′,N′*-tetra-*p*-methoxybenzyl−ethylenediamine) into a new discrete chelating metal coordination complex $[(CuCl_2)(L)]\cdot 2(H_2O)$ via a dehydrohalogenation reaction.[29] Moreover, we expanded such studies showing that the chelating complexes resulting from the mechanochemical dehydrohalogenation reaction depend on the formation of *quasi*-chelating hydrogen-bonding salts. The length of the bidentate backbone in this family of ligands is very important for the *quasi*-chelating motif formation. In the crystal structures, we described above, only **2** formed by ligand $\mathbf{L^2}$ forms the *quasi*-chelating hydrogen-bonding motif, which reacts via dehydrochlorination reaction to form $[(CuCl_2)(L^2)]$.[37]

Increasing the length of the $-(CH_2)_n-$ (n = 3, 4) backbone ($\mathbf{L^3}$ and $\mathbf{L^4}$), crystals **3** and **10** cannot form the *quasi*-chelating hydrogen-bonding motif with $[MCl_4]^{2-}$ (i.e., most likely due to the longer N···N distance). In our previous results, we carried out the mechanochemical dehydrochlorination reaction involving $CH_3CH_2OH\subset[\mathbf{L^3}]2H^+\cdot[CuCl_4]^{2-}$, and we did not see the formation of a chelated complex.[37] Here we use a new second sphere adduct having different unit cell and guest molecule (**3**). Again using liquid-assisted grinding (LAG) of **3** in the presence of KOH did not show the formation of the chelated complex and only $\mathbf{L^3}$ and KCl were obtained (Figure S29 of the Supporting Information). This corroborates our previous results. Then we tested another complex having longer backbone chain $-(CH_2)_4-$ by using the second sphere adduct **10**. In this case, upon grinding dehydrochlorination occurs but did not form the chelated complex but pure $\mathbf{L^4}$, $CdCl_2$, and KCl in its crystalline form (Figure 12).

Molecular Modeling Results. The combination of experimental and theoretical calculations (using also methods specific for solid phases) can provide complementary insights in the rationalization of solid-state reactions. Density functional theory (DFT) approaches have been employed herein. The PBE (Perdew−Burke−Ernzerhof)[43,44] exchange-correlation functionals, has been used both for gas and solid phases (i.e., under periodical conditions). All the calculations were carried out using the DMol^3 software.[45]

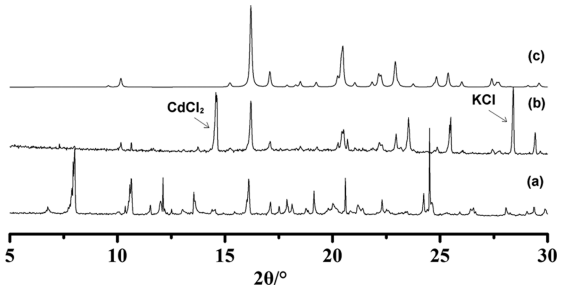

Figure 12. (a) Experimental PXRD of crystal **10**. (b) PXRD product of **10** ground in the presence of KOH (298 K). (c) PXRD pattern of ligand $\mathbf{L^4}$. It is interesting to note the formation of $CdCl_2$ and KCl as a byproduct.

A combination of numerical double-ζ quality basis set (including polarization functions on all atoms, i.e., DNP) and an effective core potential for the metal atoms was adopted. We assumed experimental X-ray determined geometries for heavy atoms while all the X−H (X = C, N, O) bond lengths were optimized because they are generally underestimated by crystal structure solution techniques. Large supramolecular complexes[46−49] systems also containing charged particles[50,51] and crystalline phases of thiophene-based oligomers and polymers[52−55] have been successfully studied using a similar computational approach. The contribution of subtle inter- and intramolecular interactions (not included in standard gradient corrected DFT algorithms) has been accounted for by the Grimme scheme within a DFT-D approach[56−58] (i.e., PBE/DNP plus Grimme corrections).

The stability of $\mathbf{L^4}$ ligand in its crystalline form has been calculated by solid phase calculations at the PBE/DNP (plus Grimme corrections) level. The sublimation energy of $\mathbf{L^4}$ is 56.8 kcal/mol, which is comparable to that of $\mathbf{L^2}$ and $\mathbf{L^3}$ molecules (60.5 kcal/mol and 51.9, respectively).

Gas phase calculations at the same level have been performed to investigate conformational energies and electron distribution of systems involved in the chelating reactions. First of all, it should be underlined once more that in $\mathbf{L^2}$, $\mathbf{L^3}$, and $\mathbf{L^4}$, the low-energy ligand structures possess different N−N distances both in crystal structures and in optimized geometries. In addition, the conformational freedom introduced by one or more extra methylene groups has a strong influence in cyclic intermediate transition states involved in the possible chelating reactions.

DFT-D calculations show that $\mathbf{L^4}$ ligand has a proton affinity (i.e., the difference in energy between neutral and protonated ligand) similar to that of $\mathbf{L^3}$ molecules (433 kcal/mol): 411 kcal/mol in **8** and 426 kcal/mol in **10**. Thus, as in the case of $\mathbf{L^2}$, in principle $\mathbf{L^4}$ can form complexes with metals as the $\mathbf{L^1}$ ligand (which has a lower estimated proton affinity, 384 kcal/mol).[37] It is interesting to note that after deprotonation, $\mathbf{L^4}$ ligands have an energy 2 kcal/mol higher with respect to the corresponding neutral molecules in the $\mathbf{L^4}$ crystal, demonstrating the scarce tendency to form a chelate system (as $\mathbf{L^1}$ does) to lower its energy.

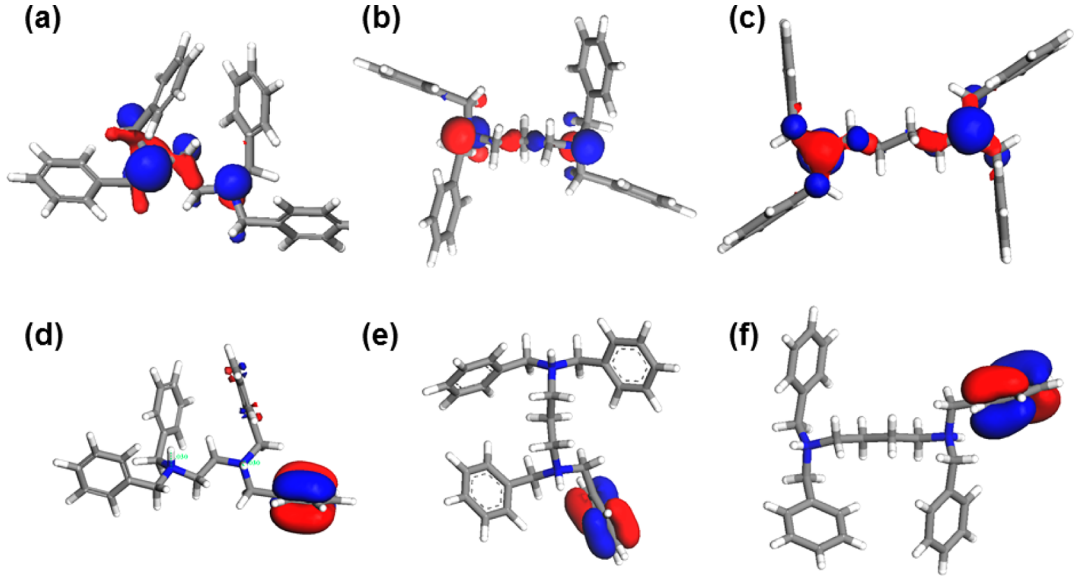

Figure 13. Structures showing the calculated HOMOs in ligands (a) $\mathbf{L}^2$, (b) $\mathbf{L}^3$, and (c) $\mathbf{L}^4$. View of the HOMOs after protonation in ligands (d) $\mathbf{L}^2$, (e) $\mathbf{L}^3$, and (f) $\mathbf{L}^4$.

Furthermore, the interactions involved in H-bonded crystals have been analyzed by calculations on small clusters of particles extracted from the single crystal X-ray structures. The interaction energy of the dimer involving protonated $[\mathbf{L}^4]\mathbf{2H}^+$ and a dianion (i.e., one forming charge-assisted H-bond) is about 252 kcal/mol in **8** and 261 kcal/mol in **10**. These interaction energies, although lower, are comparable to that observed in the $\mathbf{L}^3$ system (272 kcal/mol).[37] Therefore, protonated $\mathbf{L}^4$ forms (at least locally) stronger H-bond interactions than those observed in the *quasi*-chelating motif in protonated $\mathbf{L}^2$ with an interaction energy of 158 kcal/mol for each of the charge-assisted hydrogen bonds.[37] Thus, such lower interaction energy might facilitate the disruption of the charge-assisted hydrogen bond helping the formation of the N−Cu coordination bond upon grinding in the presence of the strong KOH base.

Further analysis of DFT-D outcomes have shown that the more reactive electrons (i.e., electrons in FMOs) in the ligand $\mathbf{L}^4$ (possessing the $-N-(CH_2)_4-N-$ moiety) are mainly localized at the N atoms (Figure 12). After N protonation, the HOMO orbitals are displaced to the phenyl moieties as observed in $\mathbf{L}^2$ and $\mathbf{L}^3$ (Figure 13). It should be emphasized that even if the HOMO orbitals of $\mathbf{L}^4$ reside mainly at the N atoms, the distribution does not allow the direct formation of a chelate without a relative rotation of the N groups to orient properly the HOMO lobes. In fact, due to symmetric reasons, the lobes of the terminal N atoms have opposite signs at variance of the case of $\mathbf{L}^2$. The number of CH_2 groups between N atoms in stable conformations of $\mathbf{L}^2$, $\mathbf{L}^3$, and $\mathbf{L}^4$ not only influences the distance between them but also plays a role in the symmetry of corresponding electron density distribution of HOMOs. Both these effects corroborate the experimental outcomes, suggesting that $\mathbf{L}^3$ and $\mathbf{L}^4$ do not form the *quasi*-chelating motif that allows the formation of a chelated complex upon dehydrochlorination.[37]

CONCLUSIONS

In this article, we have synthesized a new type of inclusion compounds based on second-sphere coordination through the deliberate design of various flexible bidentate ligands. A series of ligands based on dibenzylamine have been synthesized by inserting a methylene chain $[(CH_2)_n$ $(n = 1-4)]$ between two dibenzylamine moieties. Due to the presence of the $-(CH_2)_n-$ alkyl chains between the biphenyl rings, the torsional freedom around the C−N bonds is higher the longer the backbone chain. This results in different gauche conformation or antiperiplanar conformation of the ligands, thus forming different hydrogen-bonding networks. In addition, the influence of the $-(CH_2)_n-$ spacer length can have an effect on the inclusion property during the formation of second sphere coordination complexes. The complexes showing a reliable hydrogen-bonding motif are those with $\mathbf{L}^2$ in which the *quasi*-chelating motif between $\mathbf{L}^2$ and $[MCl_4]^{2-}$ is formed. Second sphere adducts self-assembled using diprotonated $\mathbf{L}^3$ and $\mathbf{L}^4$ with $[MCl_4]^{2-}$ have shown a great diversity of crystal structures. The second sphere adducts formed by the longest $-(CH_2)_4-$ chain ($\mathbf{L}^4$) and $[MCl_4]^{2-}$ dianion have to use guest molecules connecting $\mathbf{L}^4$ and $[MCl_4]^{2-}$ dianion and show dynamic guest uptake/release properties including crystalline-to-amorphous-to crystalline-transformations. Quantum mechanical calculations have shown that dehydrohalogenation reactions seem to occur only when there is a good size matching between the diprotonated N in the cation and the dianions. But not only size matching between reactants is important but also intermolecular interactions, conformational energies, and the symmetry of frontier molecular orbitals play a crucial role.

We believe that the strategy to synthesize new supramolecular second sphere adducts described in this work can be used to open a new family of host−guest compounds. The new second sphere adducts could find potential applications in various fields of materials science such as ion sequestration and gas adsorption. A better knowledge in their solid-state chemistry is needed to tune structure−function properties in the development of new functional materials. QM calculations can give an important input in such understanding.

ASSOCIATED CONTENT

Supporting Information

Details on the synthesis, mechanochemical reactions, comparison of experimental and simulated PXRD patterns for crystals, molar ratio, and crystallographic information. This material is available free of charge via Internet. The Supporting Information is available free of charge on the ACS Publications website.

* Notes

The authors declare no competing financial interest.

ACKNOWLEDGMENTS

This research was supported by NSFC (Grants 20903052 and 20772054), the program for Liaoning excellent talents in University (Grant LJQ 2011003), innovative team project of education department of Liaoning Province (Grant LT2011001), and 211 project of Liaoning University. A.F. acknowledges CINECA for the computational resources through a LISA Initiative (project SIMFO) and PRIN for financial support (project 2010XLLNM3_007).

REFERENCES

(1) Schmidt, G. M. H. *Pure Appl. Chem.* **1971**, *27*, 647−678.
(2) Tanaka, K.; Toda, F. *Chem. Rev.* **2000**, *100*, 1025−1074.
(3) Kole, G. K.; Vittal, J. J. *Chem. Soc. Rev.* **2013**, *42*, 1755−1775.
(4) Naumov, P. Chemical X−Ray Photodiffraction: Principles, Examples, and Perspectives. *Top. Curr. Chem.* **2012**, *315*, 111−132.
(5) Meazza, L.; Martí-Rujas, J.; Metrangolo, P.; Terraneo, G.; Resnati, G. *CrystEngComm* **2011**, *13*, 4427−4435.
(6) Martí-Rujas, J.; Meazza, L.; Lim, G. K.; Terraneo, G.; Pilati, T.; Harris, K. D. M.; Metrangolo, P.; Resnati, G. *Angew. Chem., Int. Ed.* **2013**, *52*, 13444−13448.
(7) Garai, M.; Santra, R.; Biradha, K. *Angew. Chem., Int. Ed.* **2013**, *52*, 5548−5551.
(8) Peuronen, A.; Valkonen, A.; Kortelainen, M.; Rissanen, K.; Lahtinen, M. *Cryst. Growth Des.* **2012**, *12*, 4157−4169.
(9) Martí-Rujas, J.; Kawano, M. *Acc. Chem. Res.* **2013**, *46*, 493−505.
(10) Li, C. P.; Chen, J.; Liu, C. S.; Du, M. *Chem. Commun.* **2015**, *51*, 2768−2781.
(11) Desiraju, G. R.; Vittal, J. J.; Ramanan, A. *Crystal Engineering: A Textbook*; World Scientific: Singapore, 2011.
(12) Desiraju, G. R. *J. Am. Chem. Soc.* **2013**, *135*, 9952−9967.
(13) Liu, Z.; Schneebeli, S. T.; Stoddart, J. F. *Chimia* **2014**, *68*, 315−320.
(14) Coulquhoun, H. M.; Lewis, D. F.; Stoddart, J. F.; Williams, D. J. *Dalton Trans.* **1983**, *4*, 607−613.
(15) Colquhoun, H. M.; Doughty, S. M.; Stoddart, J. F.; Williams, D. J. *Angew. Chem., Int. Ed. Engl.* **1984**, *23*, 235−236.
(16) Alston, D. R.; Slawin, A. M. Z.; Stoddart, J. F.; Williams, D. J. *Angew. Chem., Int. Ed. Engl.* **1985**, *24*, 786−787.
(17) Colquhoun, H. M.; Stoddart, J. F.; Williams, D. J. *Angew. Chem., Int. Ed. Engl.* **1986**, *25*, 487−507.
(18) Loeb, S. J. In *Comprehensive Supramolecular Chemistry*; Atwood, J. L.; Davies, J. E. D.; MacNicol, D. D. Vögtle, F., Eds.; Elsevier Science: New York, 1996; Vol. *1*, pp 733.
(19) Beauchamp, D. A. S.; Loeb, J. *Chem.—Eur. J.* **2002**, *8*, 5084−5088.
(20) Mercer, D. J.; Loeb, S. J. *Chem. Soc. Rev.* **2010**, *39*, 3612−3620.
(21) Fyfe, M. C. T.; Glink, P. T.; Menzer, S.; Stoddart, J. F.; White, A. J. P.; Williams, D. J. *Angew. Chem., Int. Ed.* **1997**, *36*, 2068−2071.
(22) Sherman, S. E.; Lippard, S. J. *Chem. Rev.* **1987**, *87*, 1153−1181.
(23) Dalrymple, S. A.; Shimizu, G. K. H. *J. Am. Chem. Soc.* **2007**, *129*, 12114−12115.
(24) Warr, R. J.; Westra, A. N.; Bell, K. J.; Chartres, J.; Ellis, R.; Tong, C.; Simmance, T. G.; Gadzhieva, A.; Blake, A. J.; Tasker, P. A.; Schröder, M. *Chem.—Eur. J.* **2009**, *15*, 4836−4850.
(25) Turkington, J. R.; Cocalia, V.; Kendall, K.; Morrison, C. A.; Richardson, P.; Sassi, T.; Tasker, P. A.; Bailey, P. J.; Sole, K. C. *Inorg. Chem.* **2012**, *51*, 12805−12819.
(26) Forgan, R. S.; Roach, B. D.; Wood, P. A.; White, F. J.; Campbell, J.; Henderson, D. K.; Kamenetzky, E.; McAllister, F. E.; Parsons, S.; Pidcock, E. *Inorg. Chem.* **2011**, *50*, 4515−4522.
(27) Ellis, R. J.; Chartres, J.; Sole, K. C.; Simmance, T. G.; Tong, C. C.; White, F. J.; Schröder, M.; Tasker, P. A. *Chem. Commun.* **2009**, *5*, 583−585.
(28) Liu, Z.; Frasconi, M.; Lei, J.; Brown, Z. J.; Zhu, Z.; Cao, D.; Iehl, J.; Liu, G.; Fahrenbach, A. C.; Farha, O. K.; Hupp, J. T.; Mirkin, C. A.; Botros, Y. Y.; Stoddart, J. F. *Nat. Commun.* **2013**, *4*, 1855−1864.
(29) Guo, F.; Shao, H. D.; Yang, Q.; Famulari, A.; Martí-Rujas, J. *CrystEngComm* **2014**, *16*, 969−973.
(30) Martí-Rujas, J.; Cametti, M. *New. J. Chem.* **2014**, *38*, 1385−1388.
(31) Li, L.; Maddalena, F.; Oliveros, M.; Caironi, M.; Guo, F.; Martí-Rujas, J. *CrystEngComm* **2014**, *16*, 10888−10892.
(32) Abate, A.; Martí-Rujas, J.; Metrangolo, P.; Pilati, T.; Resnati, G.; Terraneo, G. *Cryst. Growth Des.* **2011**, *11*, 4220−4226.
(33) Pigge, F. C. *CrystEngComm* **2011**, *13*, 1733−1748.
(34) Weber, E. Shape and Symmetry in the Design of New Hosts. In *Solid-State Supramolecular Chemistry: Crystal Engineering*; Comprehensive Supramolecular Chemistry; MacNicol, D. D.; Toda, F.; Bishop, R., Eds.; Pergamon Press: Oxford, 1996; Vol. *6*, Ch. 17, pp 535−592.
(35) Li, L.; Fu, Y.-Q.; Guo, F.; Gao, J.; Tong, J.; Zhou, Z.-F. *RSC Adv.* **2013**, *3*, 11594−11600.
(36) Pan, Z.; Zhang, M.; Yuan, D.; Ma, P. *Acta Crystallogr.* **2005**, *E61*, o185−o186.
(37) Guan, H. Y.; Wang, Z.; Famulari, A.; Wang, X.; Guo, F.; Martí-Rujas, J. *Inorg. Chem.* **2014**, *53*, 7438−7445.
(38) Ohara, K.; Martí-Rujas, J.; Haneda, T.; Kawano, M.; Hashizume, D.; Izumi, F.; Fujita, M. *J. Am. Chem. Soc.* **2009**, *131*, 3860−3861.
(39) Martí-Rujas, J.; Islam, N.; Hashizume, D.; Izumi, F.; Fujita, M.; Kawano, M. *J. Am. Chem. Soc.* **2011**, *133*, 5853−5860.
(40) Bennett, T. D.; Cheetham, A. K. *Acc. Chem. Res.* **2014**, *47*, 1555−1562.
(41) Espallargas, G. M.; Brammer, L.; Van de Streek, J.; Shankland, K.; Florence, A. J.; Adams, H. *J. Am. Chem. Soc.* **2006**, *128*, 9584−9585.
(42) Adams, C. J.; Colquhoun, H. M.; Crawford, P. C.; Lusi, M.; Orpen, A. G. *Angew. Chem., Int. Ed.* **2007**, *46*, 1124−1128.
(43) Perdew, J. P.; Burke, K.; Ernzerhof, M. *Phys. Rev. Lett.* **1996**, *77*, 3865−3868.
(44) Perdew, J. P.; Burke, K.; Ernzerhof, M. *Phys. Rev. Lett.* **1997**, *78*, 1396−1396.
(45) Delley, B. *J. Chem. Phys.* **2000**, *113*, 7756.
(46) Kolokoltsev, Y.; Amelines-Sarria, O.; Gromovoy, T. Y.; Basiuk, V. A. *J. Comput. Theor. Nanosci.* **2010**, *7*, 1095−1103.
(47) Amelines-Sarria, O.; Kolokoltsev, Y.; Basiuk, V. A. *J. Comput. Theor. Nanosci.* **2010**, *7*, 1996−2003.
(48) Basiuk, V. A.; Amelines-Sarria, O.; Kolokoltsev, Y. *J. Comput. Theor. Nanosci.* **2010**, *7*, 2322−2330.
(49) Basiuk, V. A. *Int. J. Quantum Chem.* **2011**, *15*, 4197−4205.
(50) Yu, G.; Yin, S.; Liu, Y.; Shuai, Z.; Zhu, D. *J. Am. Chem. Soc.* **2003**, *125*, 14816−14824.
(51) Maccaroni, E.; Malpezzi, L.; Famulari, A.; Masciocchi, N. *J. Pharm. Biomed. Anal.* **2012**, *60*, 65−70.
(52) Famulari, A.; Raos, G.; Baggioli, A.; Casalegno, M.; Po, R.; Meille, S. V. *J. Phys. Chem. B* **2012**, *116*, 14504−14509.
(53) Guo, F.; Zhang, M.-Q.; Famulari, A.; Martí-Rujas, J. *CrystEngComm* **2013**, *15*, 6237−6243.

(54) Nicolini, T.; Famulari, A.; Gatti, T.; Martí-Rujas, J.; Villafiorita Monteleone, F.; Canesi, E. V.; Botta, C.; Parisini, E.; Meille, S. V.; Bertarelli, C. *J. Phys. Chem. Lett.* **2014**, *5*, 2171−2176.
(55) Casalegno, M.; Baggioli, A.; Famulari, A. Meille, S. V.; Nicolini, T.; Po, R.; Raos. G. *Materials for organic photovoltaics: Insights from detailed structural models and molecular simulations*; EPJ Web of Conferences; 02002-1 02002-8; 2012, ISSN 1528-7483, DOI: 10.1051/epjconf/20123302002.
(56) Grimme, S. *J. Chem. Phys.* **2006**, *124*, 34108−34134.
(57) Baggioli, A.; Meille, S. V.; Raos, G.; Po, R.; Brinkmann, M.; Famulari, A. *Int. J. Quantum Chem.* **2013**, *113*, 2154−2162.
(58) Baggioli, A.; Famulari, A. *Phys. Chem. Chem. Phys.* **2014**, *16*, 3983−3994.